Greenhouse Gas Emissions and Dispersion

3. Reducing Uncertainty in Estimating Source Strength and Location through Plume Inversion Models

Kuldeep Prasad
Adam Pintar
Heming Hu
Israel Lopez-Coto
Dennis Ngo
James Whetstone

NIST

National Institute of Standards and Technology
U.S. Department of Commerce

Greenhouse Gas Emissions and Dispersion

3. Reducing Uncertainty in Estimating Source Strength and Location through Plume Inversion Models

Kuldeep Prasad
Heming Hu
Israel Lopez-Coto
Dennis Ngo
NIST Engineering Laboratory

Adam Pintar
Statistical Engineering Division

James R. Whetstone
NIST Office of Special Programs

September 2015

U.S. Department of Commerce
Penny Pritzker, Secretary

National Institute of Standards and Technology
Willie May, Under Secretary of Commerce for Standards and Technology and Director

Greenhouse Gas Emissions and Dispersion
3. Reducing Uncertainty in Estimating Source Strength and Location through Plume Inversion Models

Kuldeep Prasad, Adam Pintar, Heming Hu, Israel Lopez-Coto, Dennis Ngo,
James Whetstone

Abstract

Recent development of accurate instruments for measuring greenhouse gas concentrations and the ability to mount them in ground-based vehicles has provided an opportunity to make temporally and spatially resolved measurements in the vicinity of suspected source locations, and for subsequently estimating the source location and strength. The basic approach of using downwind atmospheric measurements in an inversion methodology to predict the source strength and location is an ill-posed problem and results in large uncertainty. In this report, we present a new measurement methodology for reducing the uncertainty in predicting source strength from downwind measurements associated with inverse modeling. In order to demonstrate the approach, an inversion methodology built around a plume dispersion model is developed. Synthetic data derived from an assumed source distribution is used to compare and contrast the predicted source strength and location. The effect of introducing various levels of noise in the synthetic data or uncertainty in meteorological variables on the inversion methodology is studied. Results indicate that the use of noisy measurement data had a small effect on the total predicted source strength, but gave rise to several spurious sources (in many cases 8-10 sources were detected, while the assumed source distribution only consisted of 2 sources). Use of noisy measurement data for inversion also introduced large uncertainty in the location of the predicted sources. A mathematical model for estimating an upper bound on the uncertainty, and a bootstrap statistical approach for determining the variability in the predicted source distribution is demonstrated. The new measurement methodology, which involves using measurement data from two or more wind directions, combined together as part of a single inversion process is presented. Results of the bootstrap process indicated that the uncertainty in locating sources reduced significantly when measurements are made using the new proposed measurement approach. The proposed measurement system can be significant in determining emission inventories in urban domains at a high level of reliability, and for studying the role of remediation measures.

1 Introduction

There has been renewed interest in recent years, in using inverse atmospheric dispersion methods as part of a top-down analysis, to estimate the source location and strength of greenhouse gas (GHG) emissions [1]-[16]. Development of accurate instruments [17]-[19] for measuring temporally resolved greenhouse gas concentrations and the ability to mount them in mobile vans, airplanes and towers has enabled us to conduct such inversion analysis. However, the basic approach of using atmospheric measurements to locate and characterize sources (the inverse problem) is an inherently ill-posed problem, and can lead to large uncertainty in the predicted results. In this paper, we present sources of uncertainty in inversion analysis, quantify the error, and put forward a measurement methodology for reducing the uncertainty in estimating emissions.

Methods for estimating source strength and/or location from measurements of concentration can be divided into two major categories depending on the physical scale of the problem. For urban, regional, or continental scale inversions, researchers [1]-[7] have used ground-based observations and a high-resolution mesoscale atmospheric transport model to determine greenhouse gas emissions. They combine prior emission inventories and atmospheric observations using a Bayesian statistical

approach to estimate the emissions and the corresponding uncertainty. Enting et al. [9] has reported that characterizing and calculating the uncertainties in emissions at regional scale is difficult, and that the uncertainty structure in space and time is difficult to interpret. When the physical distance between the sources and sensor measurements are smaller, it becomes difficult to use the mesoscale atmospheric transport models for inversion. Typical examples include measurements made with instruments mounted inside ground-based vehicles operating on roads close to a possible source. For such scales atmospheric inversions are usually done using plume dispersion and surface layer models [10],[11],[12]. In this report, we are primarily interested in measurements that are made relatively close to the source and restrict ourselves to studying the uncertainty in inverse modeling related to plume dispersion models. A large number of inversion studies based on plume inversion models have appeared in the literature. A few of these studies that deal with uncertainty estimates are discussed below.

Lushi et al. used a Gaussian plume model to provide inverse estimates of particulate emissions [14]. They added artificial, randomly generated noise to their measurements at levels of ± 30 % of the measured values and found that the introduction of noise had little effect on the estimates of source strength. It was speculated that the positive and negative contributions of noise tend to cancel out its effect [14]. Their approach does not exhibit the high levels of sensitivity normally found in ill-conditioned problems, and this was attributed to the fact that measurement locations were close to the sources (< 1 km). Using monthly deposition data for the inverse estimates, aggregate (year long) estimates were within 10%-20% of reported emissions. However, large variations in monthly output were estimated and these variations were ascribed to errors in the measurement data, and the fact that detailed meteorological data for assessing atmospheric stability were not available. Lushi et al. (unlike the focus of the current study) did not investigate the sources of uncertainty in their predicted source distribution, nor did they put forth an approach for reducing the uncertainty. The result of our current research study show that noisy measurement data can have a large effect on the predicted source strength and location, a result that contradicts the work reported by [14].

Jeong et al. [15] have reported experiments in which sulfur hexafluoride (SF_6) was released at strengths of 110 kg/h to 115 kg/h from a single point source at 57 m above ground level near a nuclear power plant. Measurements were made at various heights and at two downwind distance (3 km and 8 km) from the source. Atmospheric conditions were moderately unstable during both trials comprising the experiment. They subsequently employed an inversion technique based on the Gaussian plume model; however, only source strengths, not locations, were estimated. Despite the fact that the source location was known, source strengths were overestimated by about 47 % using data from only the 3 km arc, and by about 72 % when data from only the 8 km arc were used [15]. The experiments reported by Jeong et al. provide a useful way to test the inversion method. Although they report some uncertainty in the predicted results, Jeong et al. did not investigate the source of this uncertainty, nor did they provide a scientific basis for reducing or managing the uncertainty in their predicted results.

Finally, Rudd et al. [16], studied the sensitivities of predicting source strength *and location* to the number of downwind sensors, sensor configuration, averaging time and noise in the input data. Data from wind tunnel experiments, in which a tracer gas (propane) was released into the air from a single source location, were used to test their inverse model. Using data from the wind tunnel experiment, dispersion coefficients and wind speed necessary in the Gaussian plume model were customized to provide the best possible model of downwind concentrations. Rudd et al. estimated that the Gaussian plume model introduced an error of 1.5 ppmv into estimates of downwind concentration when the wind tunnel experiment was assumed to have a scale of 1:500, corresponding to a reference wind speed of 10 m s^{-1} at 32 m, a boundary layer height of 500 m and

a source strength of 0.1 m³ s⁻¹ [16]. It was noted that uncertainties in wind speed and dispersion coefficients will be greater in field applications than in the controlled wind tunnel experiment, and therefore greater model error would be expected [16].

The literature review presented above clearly shows that plume dispersion models have been used extensively for estimating the source strength and location from various tracer release experiments. Researchers also reported large uncertainty in their inverse estimates, but have provided limited explanation for the observed uncertainties. In this report, we use synthetic data to understand the sources of the uncertainty in plume inversion models. There has been limited research on developing methods for reducing the uncertainties and for studying the variability of the source distribution. The goal of this report is to propose a new measurement methodology for reducing the uncertainty in inversion analysis.

In Section 2, we provide a brief description of the physical problem and provide the basic mathematical framework of an inverse problem. Governing equations for the plume dispersion model are presented and the numerical methods for solving the inversion problem are discussed. Section 3 provides a description of the basic source - sensor configuration that is used to test the ideal (base-case) inversion problem. Several sources of uncertainty such as noise in the measurement data, lack of accurate information on wind speed and direction, as well as atmospheric stability conditions are explored, and their effect on inversion are quantified. Section 4 presents a methodology for estimating the upper bound on the uncertainty in inversion, while section 5.1 provides an approach for quantifying the variability in predicting source strength and location. Finally, section 6 presents a measurement approach for reducing the uncertainty in inversion. We conclude by providing suggestion for incorporating the new measurement approach into future mobile campaigns for estimating emission inventories.

2 Model Formulation and Description of the Problem

Consider a source of known strength Q (kg s⁻¹) that is releasing a tracer gas into the atmosphere. We also assume that a sensor is located downwind of the source, where we need to estimate the concentration of the tracer gas. The concentration C (measured in kg m⁻³) of the tracer gas at the sensor location can be modeled using the equation

$$\left(\frac{C}{Q}\right)_{est} Q + C_{bg} = C \tag{1}$$

where C_{bg} is the background concentration, and $(C/Q)_{est}$, represents the influence of the source on the sensor (influence function). This ratio can be estimated from a variety of models such as plume models, computational fluid dynamics models or from tracer experiments. The difficulty in this seemingly trivial model lies in obtaining an accurate value of the ratio $(C/Q)_{est}$ for the given configuration of source and measurement point.

2.1 Estimating source strength and location - the inverse problem

The inverse of this problem occurs when concentrations are known, but source strengths, or their locations, are not. In the above model, a single source strength could be estimated from a single measurement simply by solving for Q in Equation 1.

$$Q = \frac{C - C_{bg}}{\left(\frac{C}{Q}\right)_{est}} \tag{2}$$

4

Note, that the predicted source strength is a function of the *reciprocal* of the estimated ratio, $(C/Q)_{est}$. Thus, small changes (errors) in the estimated ratio may produce large changes in the inverse estimate of Q.

The problem becomes more complicated when multiple sources and measurements are involved. For n sources that generate concentrations measured at m locations, the necessary set of equations may be written as [11]:

$$
\begin{pmatrix}
\frac{C_{1,1}}{Q_1} & \frac{C_{1,2}}{Q_2} & \cdots & \frac{C_{1,n}}{Q_n} \\
\frac{C_{2,1}}{Q_1} & \frac{C_{2,2}}{Q_2} & \cdots & \frac{C_{2,n}}{Q_n} \\
\vdots & \vdots & \ddots & \vdots \\
\frac{C_{m,1}}{Q_1} & \frac{C_{m,2}}{Q_2} & \cdots & \frac{C_{m,n}}{Q_n}
\end{pmatrix}_{est}
\begin{pmatrix}
Q_1 \\ Q_2 \\ \vdots \\ Q_n
\end{pmatrix}
+
\begin{pmatrix}
C_1 \\ C_2 \\ \vdots \\ C_m
\end{pmatrix}_{bg}
=
\begin{pmatrix}
C_1 \\ C_2 \\ \vdots \\ C_m
\end{pmatrix},
\tag{3}
$$

where for visual clarity, the subscript "est" has been applied to the entire matrix instead of its individual elements. Equation 3 may be written in a more compact notational form as

$$
\mathbf{G}\mathbf{Q} + \mathbf{C}_{bg} = \mathbf{C},
\tag{4}
$$

where $\mathbf{G}$ represents a matrix of the estimated ratio terms $(\frac{C}{Q})_{est}$, $\mathbf{Q}$ represents a vector of the source terms, and $\mathbf{C}_{bg}$ and $\mathbf{C}$ represent the vector of background concentrations and the sensor measurement, respectively.

The challenge of the inverse problem however, lies in the fact that the coefficient matrix $\mathbf{G}$ is usually ill-conditioned for physically realistic scenarios, rendering the inverse problem extremely sensitive to very small changes in concentration measurements as well as error introduced by the dispersion model [8]. Any model relating source strength to downwind concentration could be used to calculate the elements of $\mathbf{G}$ and to subsequently conduct an inverse analysis. Since the purpose of this report is to identify the sources of uncertainty in inversion analysis, and to develop a methodology for reducing this uncertainty, we use a simple plume model to construct the inversion matrix, so that computations can be carried out in a quick and efficient manner. It should be pointed out that the predicted source strengths will be sensitive to errors introduced in the analysis, irrespective of the choice of the actual model that is used to construct the elements of the inversion matrix because of the ill-conditioned nature of the inversion matrix $\mathbf{G}$.

2.2 Gaussian plume model

The time-evolution of the concentration of a passive, conserved scalar in the atmosphere may be modeled as a diffusion equation:

$$
\frac{\partial C(x,y,z,t)}{\partial t} = K_{x,y,z}\nabla^2 C(x,y,z,t),
\tag{5}
$$

where t is time, and the diffusion coefficients, $K_{x,y,z}$, represent turbulent (eddy) diffusivity rather than molecular diffusion Assuming the source strength, Q, as a forcing term, a solution to this equation in a cartesian coordinate system was provided by Ermak et al. [20]

$$
\frac{C(x,y,z)}{Q} = \frac{1}{2\pi u \sigma_y \sigma_z} \exp\left(-\frac{1}{2}\left(\frac{y}{\sigma_y}\right)^2\right)\left[\exp\left(-\frac{1}{2}\left(\frac{z-H}{\sigma_z}\right)^2\right) + \exp\left(-\frac{1}{2}\left(\frac{z+H}{\sigma_z}\right)^2\right)\right],
\tag{6}
$$

where u is the mean streamwise wind speed; σ_y and σ_z (m) are *dispersion* coefficients in the crosswind and vertical directions, respectively, y is crosswind distance from the plume centerline

5

(m), z is height above ground (m) and H is the height of the source (m). This form of the plume model (Equation 6) includes the portion of the plume "reflected" from the ground (2nd term in the large brackets).

The diffusion coefficients in the crosswind (K_y) and vertical (K_z) directions are related to the dispersion coefficients σ through the relation [18].

$$\sigma_y \quad = \quad \sqrt{2K_y(x/u)} \tag{7}$$

$$\sigma_z \quad = \quad \sqrt{2K_z(x/u)} \tag{8}$$

The values of the dispersion coefficients are therefore functions of streamwise (x-axis) distance, and may be estimated according to atmospheric stability and downwind distance from the source. For simplicity, we use the Pasquill-Gifford-Turner (PGT) categories which partition atmospheric stability into six groups, ranging from "A" (very unstable), to "F" (very stable). Formulas relating σ_y and σ_z to downwind distance were determined empirically for each of these classes [21], [22].

Several assumptions are made in the simple dispersion model that is proposed in this section. Emissions for the sources are assumed to be constant and continuous over time. It is also assumed that the gases or pollutants are conserved as they disperse (i.e., there is no deposition) and that they do not react with, or decay into other products. Meteorological conditions (wind speed, direction and static stability) are assumed to be constant throughout the domain and over the time that it takes for gases to be transported between sources and receptors.

2.3 Solving the inverse problem

In the inverse simulations below, we assume that source strengths are unknown and that all sources are contained somewhere within an upwind area defined and represented by a grid of points. Ratios of downwind concentration to source strength were calculated for each combination of source grid point and measurement (concentration) location using Equation 6. The values of these ratios populate the matrix in Equation 3. The dimensions of the resulting matrix are therefore m x n, where m is the number of measurement points, and n is the number of locations within the source area.

A solution to the inverse problem was estimated using the non-negative least squares (nnls) algorithm of Lawson and Hanson [23]. This numerical algorithm minimizes the norm of the difference between the left and right hand sides of Equation 3, i.e., it produces a vector, $\mathbf{Q}$, with all elements greater than or equal to zero, that minimizes $\|\mathbf{GQ} - \mathbf{C}\|$. Proof of convergence and details of the algorithm may be found in [23]- [26].

3 Basic Configuration for Predicting Source Strength and Location

The objective of this study is to estimate and reduce the uncertainty in locating the sources and their strength from downwind measurement data. In this section, we present the basic configuration of measurement locations relative to the source area, that is used in our simulations.

Figure 1 illustrates a schematic diagram, in plan view, of the configuration of sensor measurements and source area for evaluating the plume inversion model. The square area shown in Figure 1 has dimensions of 2.5 km $\times$ 2.5 km, and represents a domain where the sources are located. It is assumed that the wind direction is from left to right (parallel to the x-axis). Downwind of the source are three lines located at $x = 4000, 5000$ and 6000 m, which schematically represent the

location of the measurements. Measurement data[1] can be obtained from a variety of sources such as tower measurements, aircraft measurements or from an instrument mounted inside a vehicle. Synthetic measurements that attempt to mimic measurement made from an instrument mounted inside a vehicle can also be generated. Since the goal of this report is to estimate and reduce uncertainty in source location and strength, we employ the approach of using synthetic measurement data. The use of synthetic data has the additional advantage that we can compare the inversion results with the total known source strength as well as checking the accuracy of the location of the predicted sources. The lines in Figure 1 each indicate the location of 502 measurement points, with a total of 1506 measurements points on the three lines. Since the assumed wind direction in this ideal (base) configuration is from the West, the lines of measurement points are perpendicular to the flow. The source and measurement domains depicted in Figure 1 have been chosen to roughly match what is expected in real deployments.
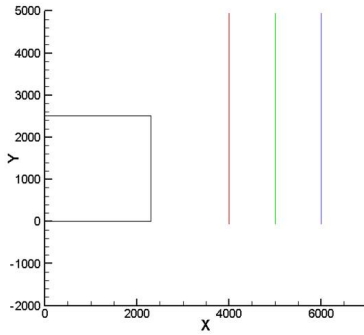
Figure 1: Plan view of source-sensor configuration that is used for estimating and reducing the uncertainty in prediction of sources and their location. The square (2.5 km × 2.5 km) represents the location of the sources, while the lines indicate an array of measurement locations downwind of the source. All units are in meters.

As discussed earlier, we assume a set of known sources (located inside the square area of Figure 1) to create synthetic data that is subsequently used in the algorithm. The location of these known (assumed) sources and their source strength are shown in detail in the surface plot (Figure 2 left sub-figure). The source area is represented as a regular grid of 40 x 37 elements (i.e., the area is resolved into 62.5 m x 67.6 m cells). The elements of the source grid are therefore represented by a vector of 1480 elements. The surface plot shows the presence of two sources; one that is located in the leftmost corner of the grid has a source strength of 0.1398 kg/s, while the other located in the rightmost corner has a source strength of 0.0975 kg/s.

The known (assumed) sources and their strength are also indicated by the bar plot on the right side of Figure 2, where they are referred to by the index number of the cells within the source area grid. The spikes shown in the bar plot represent, from left to right, source strengths of 0.1398 kg/s and 0.0975 kg/s (total = 0.2373 kg/s), respectively. Hereon, the stronger (leftmost) and weaker (rightmost) source will be referred to as sources "A" and "B," respectively. In all simulations described below, the location of the assumed sources and their strengths remained constant, while the configuration of measurement locations, the *assumed* wind direction, measurement noise and

---

[1]Certain commercial equipment, instruments, or materials are identified in this report in order to specify the experimental procedure adequately. Such identification is not intended to imply recommendation or endoresement by the National Insitute of Standards and Technology, nor is it intended to imply that the materials or equipment identified are necessarily the best available for the purpose.

atmospheric stability class were varied to study their effect on inversion.
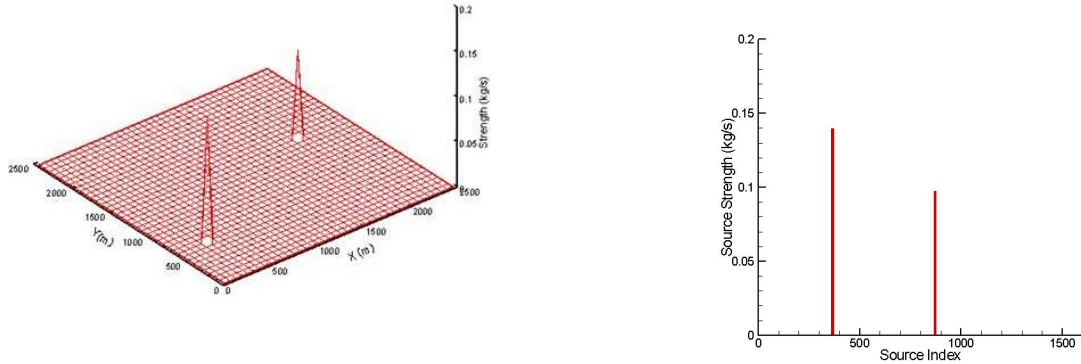
Figure 2: Surface plot (left sub-figure) and bar chart (right sub-figure) showing the location of the assumed sources and source strength measured in kg/s.

The assumed sources are used to create synthetic data at the measurement locations, as well as for comparison with the predicted source distribution. Uncertainty in the prediction can be estimated by evaluating the differences between the predicted and assumed source distribution. Qualitative comparisons can be made through comparison of the surface and bar plots shown in Figure 2. Synthetic data is generated by using the plume Equation 6 to calculate downwind concentrations at the measurement locations (illustrated by the lines in Figure 1). A wind speed of 2.5 m/s and a neutral atmospheric stability (PGT class D, urban) was assumed. The synthetic data is shown in Figure 3, which shows a 3D line plot of downwind concentrations (density measured in kg/m^3) plotted on the three measurement lines. Synthetic data at measurement lines located at x= 4000 m, 5000 m and 6000 m are shown with red, green, and blue lines, respectively. Note that the nearest line of measurement points (x = 4000 m) shows two separate peaks corresponding to the separate sources. As expected, the peak concentrations diminish with distance from the sources.
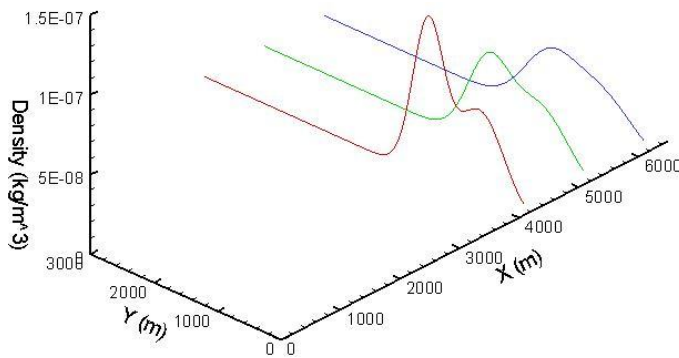
Figure 3: Synthetic data obtained at the sensor locations using the assumed source location and strength.

The synthetic data generated above is next used in an inversion framework to identify the source strength and locations. The synthetic data forms the concentration vector **C** in Equation 4; the coefficient matrix, **G** was generated from Equation 6, and the nnls algorithm (discussed in Section 2) was used to solve the inverse problem by estimating the source vector, **Q**. The predicted

source distribution **Q** obtained after inverting the matrix is shown in Figure 4. Comparison of the predicted source distribution (Figure 4) and the assumed source distribution (Figure 2) indicates that the predicted and assumed source distributions are essentially identical. The total predicted source strength was only 0.001 % greater than the assumed total source strength. The location of the predicted sources was also identical to that of the assumed sources (as seen clearly in the bar plots). Since the synthetic data was generated from the plume model, this case represent perfect inversion. This perfect inversion is a verification of the underlying algorithms that have been used and the validity of the matrix inversion process.
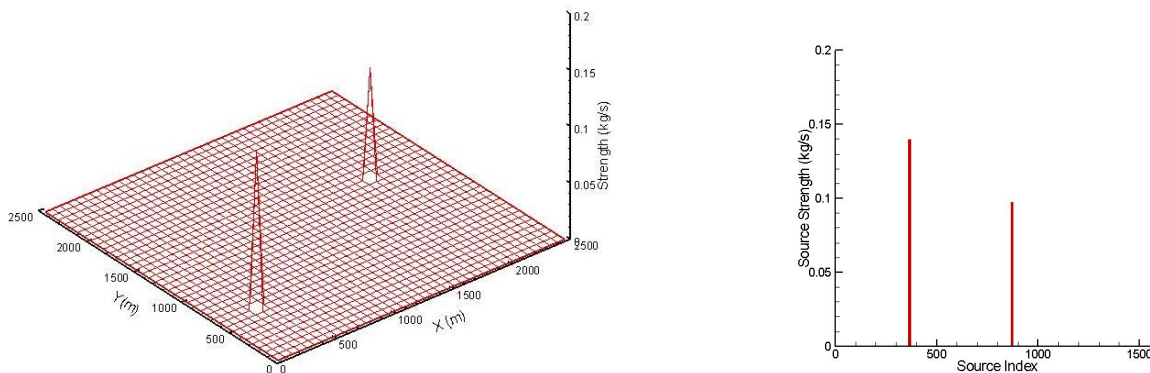
Figure 4: Surface and bar chart showing the location of the predicted sources and source strength for the base (ideal) case scenario.

3.1   Effect of measurement distance from the source area

In order to further evaluate the inversion methodology, we study the effect of moving the measurement locations further away from the source. It is well known that dispersion increases with downwind distance from the source, but it is not clear if moving the measurement locations further downwind will adversely affect the inversion results.

To study the effects of this phenomenon on the inverse estimates, the ideal case, in which the array of measurement locations began at x=4000 m, was repeated with the array moved further downwind. In three separate simulations, the array began at x=8000, 12000 and 16000 m, respectively. The distance between the rows (1000 m) array was held constant. Concentrations at each measurement location were estimated using Equation 6. These concentration values were then used in the inverse estimates to find the locations and strengths of the individual sources.

The results are illustrated in Figure 5 below, where distance to the measurement rows increases from the top to bottom of the page. The top panels are for measurements that begin at 8000 m downwind of the source, the middle two panels for 12000 m downwind of the source, and bottom panels for 16000 m from the source. The total source strength for the three cases was 0.23728 kg/s, 0.23729 kg/s and 0.23726 kg/s. Error in the estimate of total source strength was insignificant ($<< 1\%$), but it is clear from the surface and bar plots, that estimates of source locations become less accurate with increasing distance to the measurement locations.

In all three cases, multiple source locations were estimated, with a total of 13 sources in the 8000 m case, and 10 sources in each of the other two. Many of these sources were of negligible strength ($\sim 10^{-3}$ kg/s) compared to the true source strengths, and are barely, or not at all, visible on either the surface or bar plots. However, it is clear that the number of non-negligible ($\sim 10^{-1}$ kg/s) spurious sources increased with distance to the measurement locations, though these sources tend

9
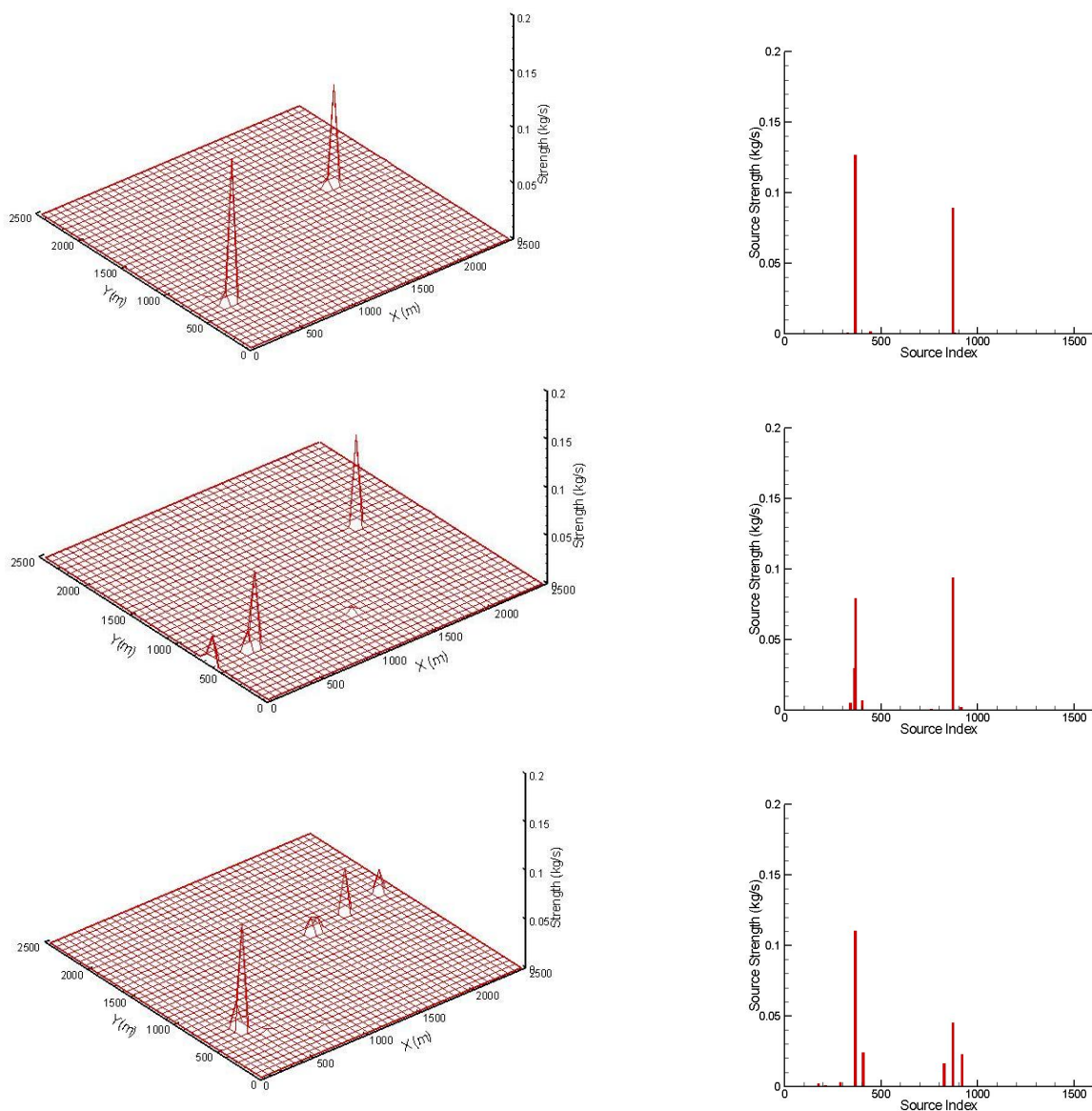
Figure 5: Inverse estimates of source strength and location when the set of measurements begins at 8000 m (top two panels), 12000 m (middle panels) and 16,000 m (bottom panels) downwind of the source area.

to be grouped relatively near the true source locations. For example, in the bottom panel of Figure 5, the inverse estimate of source B comprises four sources with a total strength approximately equal to the true strength of source B.

Since dispersion increases with downwind distance from the source, details of the combined gas plume such as the two separate peaks of the leftmost line of measurements in Figure 3 become less distinguishable with increasing distance from the sources. In effect, information that can be used to estimate separate source locations is lost with increasing downwind distance as seen in our results.

3.2 Effect of noise in measurement data

Measurements are usually collected with instruments mounted on a vehicle traversing along a road that is nominally perpendicular to the wind direction. As the vehicle path intercepts the plume, the on-board instruments record the local concentration in the plume. Since the plume itself is continuously evolving in time, the vehicle may intercept different portions of a turbulent plume at different locations. The microscopic turbulent eddies that are part of a plume can result in significant noise in the measurement data. Noise in the measurement data can also be attributed to changes in meteorological conditions during a transect. Usually data from a few transects are averaged together, but it is conceivable that this averaged concentration may not be a true representation of a Gaussian plume.

In this section, we investigate the effect of using noisy measurement data on the inverse calculation. Results are shown for two cases with different levels of noise incorporated in the measurement data. Noisy data was created by adding random variations to the downwind concentrations that were calculated in the ideal case (base case) synthetic data. The level of noise was chosen based on observations of real data from mobile campaigns [19]. At the location of each measurement, a random percentage of its concentration, taken from a uniform distribution was added to the synthetic data.
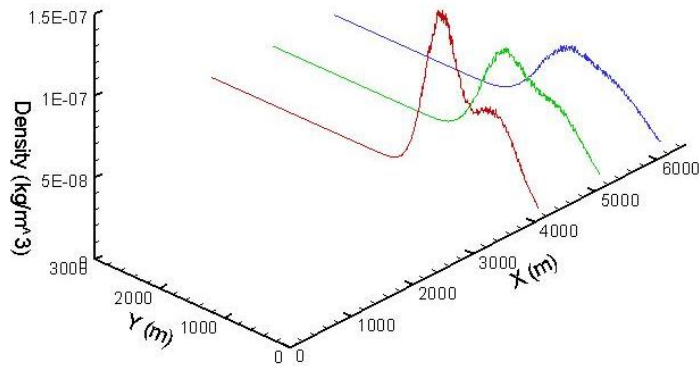
Figure 6: Synthetic data modified with 10 % noise

In the first case, 10% noise (i.e., variation of $\pm$ 5 % of the signal above the background level) was added to each of the measurement points. The synthetic data modified with 10 % noise is shown in Figure 6. The resulting effect of using the noisy data on the inverse calculation is illustrated in Figure 7, which shows surface and bar charts for the predicted source distribution. The total predicted source strength was 0.2415 kg/s, which was only about 1.8 % greater than the actual (assumed) source strength. However the surface and bar charts (Figure 7) indicated the presence of multiple sources. Results also indicate that the location of the sources was significantly different than the assumed source distribution shown in Figure 2. Estimates of *crosswind* locations were accurate for both of the sources, but the streamwise (x-axis) location of the stronger source (source A) was estimated to be at the windward edge of the source area, about 300 m upwind of the true location, and was spread over adjacent source grid locations. Overall, ten source locations were identified in the inverse calculation, though only four had values of the same order ($\sim 10^{-1}$) as the true sources.

In the second case, 30 % noise (variation of $\pm$ 15 %) was added to the downwind concentrations above the base-case levels. The modified synthetic data with 30 % noise is shown in Figure 8, while the predicted source distribution is shown in Figure 9. Despite tripling the amount of noise
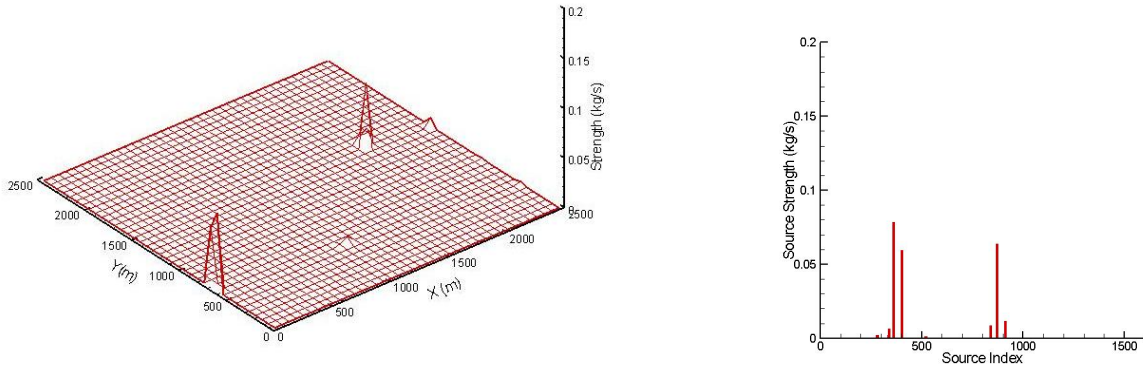
Figure 7: Predicted source distribution (surface and bar charts) for inversion of synthetic data modified with 10 % noise.

in the measurements, total source strength was overestimated by only about 3 %, but there was significant error in the location of the predicted sources. Once again, the larger source location was spread over two cells, and estimated to be at the windward edge of the domain. The sum of source strengths for these two locations (leftmost vertical red bars in the lower right panel of Figure 9) was 0.15 kg/s, an overestimate of about 8 % from the value of source A. As before, ten source locations were identified, although only five were of the same order as the true sources.
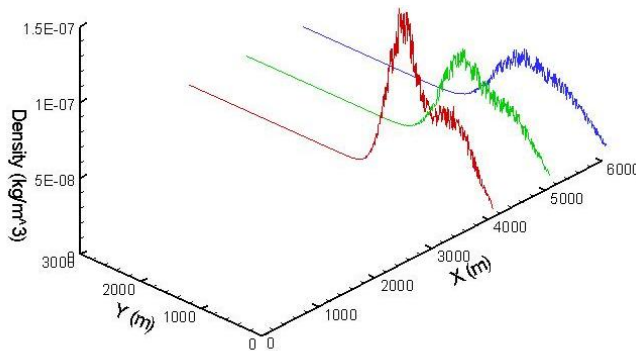
Figure 8: Synthetic data modified with 30% noise

In both of these cases, the estimated streamwise position of the source furthest from the measurement locations (source A) was most affected by the random noise added to the measurements. This is due to the fact that the measurements are much less dense in the streamwise direction, where the relevant information for the inverse estimate comes essentially from the concentration gradients between only three rows of data, rather than between closely neighboring points as in the crosswind case.

3.3   Other sources of uncertainty

The previous section demonstrated the effect of using noisy measurement data on the predicted source location and strength, following an inversion analysis. Besides noisy measurement data, there are several other sources of uncertainty that can have a direct effect on the predicted source strength and location. They include factors such as changes in meteorological conditions, such
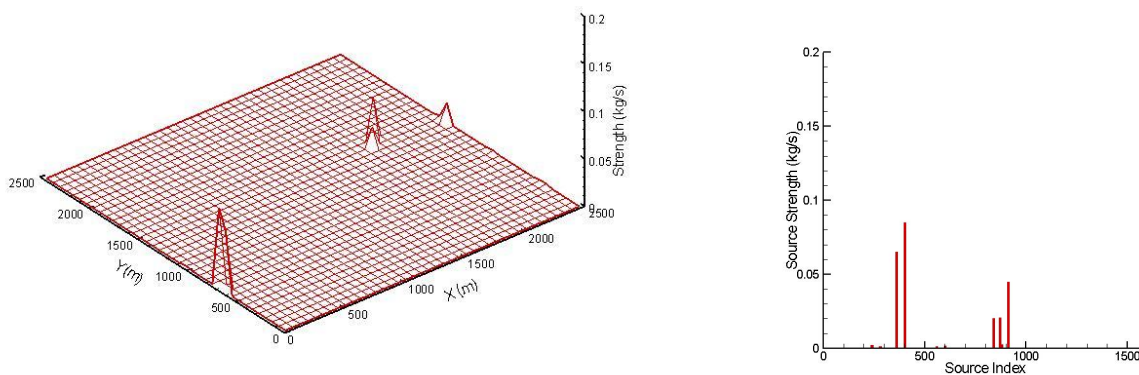
Figure 9: Predicted source distribution (surface and bar charts) for inversion of synthetic data modified with 30 % noise.

as wind speed and direction, as well as the uncertainty in the ability of the model to simulate the atmospheric conditions (atmospheric stability). In this section we demonstrate the effect of uncertainty in using incorrect wind direction information and its effect on the inversion process.

Downwind concentrations estimated by the forward dispersion model (Equations 1) are based on the assumption that mean wind direction is known to a high degree of accuracy. However, there are several sources of uncertainty in measurements of wind direction including instrument calibration errors, and accuracy and placement of anemometers or wind vanes. The latter is especially important since the mean wind direction near a source location may not be the same as that near the measurement location (instrument is located far away from the sources). A different kind of uncertainty arises when atmospheric models are used to estimate mean wind direction between sources and measurement locations.
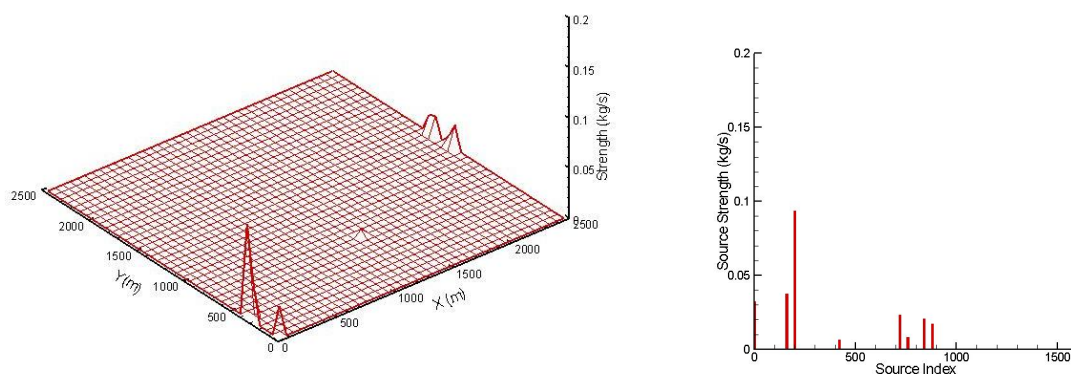

Figure 10: Effect of uncertainty in wind-direction on the predicted source strength and location. Synthetic data is created with a wind in the x-direction (270.0 °), but a wind direction of 265.0 ° is assumed during the inversion process.

We report two specific calculations that were conducted to understand and evaluate the effect of using an incorrect wind-direction vector in the inversion algorithm. Downwind concentrations from the ideal case, in which wind direction was parallel to the x-axis, were used in both cases. However, in the first case, the terms of the inversion matrix $\mathbf{G}$ were computed by assuming that the wind direction was in-correctly estimated to be 5° counter-clockwise (CCW) from the original

13

direction (i.e., from the x-axis). Figure 10 shows the predicted source strength and location when wind direction was assumed to be 5° counter-clockwise (CCW) from the x-axis. The error in the wind direction had little effect on the estimate of total source strength, with an overestimate of only 0.6 %, but it is clear from Figure 10 that the locations and strengths of the individual sources were not well-characterized. Figure 11 shows the source strength and location when wind direction was in error by 5° clockwise (CW) from the original direction. In this case, the total source strength was underestimated by 3.4 %, but the estimated locations of the individual sources again departed significantly from the true locations.
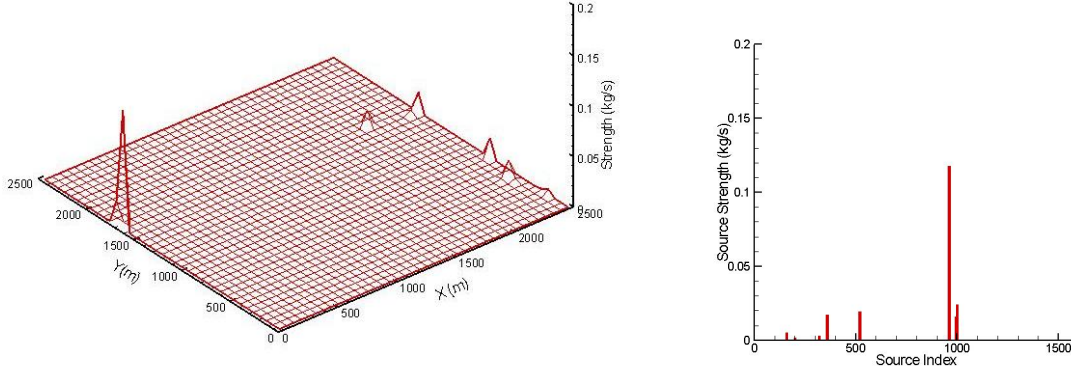
Figure 11: Effect of error in wind-direction on the predicted source strength and location. Synthetic data is created with a wind in the x-direction (270.0 °), but a wind direction of 275.0 ° is assumed during the inversion process.

The asymmetry in the estimates of source strength for the two cases reflects the lack of symmetry around the x-axis in the true source *and measurement* locations. Relative to the true source locations, the rows of measurement points extend further in the positive y-axis direction than in the negative (see Figure 1). Inspite of this asymmetry, these cases illustrate the strong effect of error in wind direction on the *location* of individual sources within the estimated source area. However, the results also suggest that total source strength can be estimated with reasonable accuracy as long as the measurement field intersects the majority of the plume.

4   Upper Bound on Uncertainty in Source Strength

In the previous section, we have presented several examples that demonstrate the uncertainty in predictions of source strength and location attributed to noisy measurement data or incorrect meteorological data. This uncertainty in prediction of source strength and location can be mathematical quantified through the concept of condition number.

In order to predict emission from downwind measurement data, the system of linear Equations 4 are inverted. The relative error, or uncertainty, in the calculation of source strength can be written mathematically as

$$\frac{\|\Delta \mathbf{Q}\|}{\|\mathbf{Q}\|} \leq \kappa \quad \frac{\|\Delta \mathbf{G}\|}{\|\mathbf{G}\|} + \frac{\|\Delta \mathbf{C}\|}{\|\mathbf{C}\|} + \frac{\|\Delta \mathbf{C_{bg}}\|}{\|\mathbf{C_{bg}}\|} \tag{9}$$

where Δ signifies a change or error, the operator $\| \cdot \|$ represents a norm (usually the Euclidean or spectral norm), and κ indicates the *condition number* [10]. If $\mathbf{G}$ is square (i.e., $m = n$) and non-singular, the condition number κ may be calculated as $\|\mathbf{G}\|/\|\mathbf{G}^{-1}\|$. For rectangular matrices

14

$(m \neq n)$, the condition number may be calculated as the ratio of the largest and smallest singular values [26].

Equation 9 provides an upper bound on the relative error in the estimated source strength. This relative error is proportional to the condition number κ, as well as the relative error in estimating the coefficient matrix, the measured concentrations and background concentrations [10][25]. Therefore, a low value of κ implies a low sensitivity to error, but a large value does not necessarily imply a high sensitivity. The uncertainty in source strength increases, if the configuration of measurement locations and sources is ill-posed and is reflected in large values of the condition number.

For the ideal case shown in Section 3, the condition number of the coefficient matrix was calculated to be 2.87×10^{26}. Inspite of the large value for the condition number, the errors in the inversion process were found to be extremely small (Figure 4). This is due to the fact that the uncertainties in the (prescribed) background concentration, "measurements," and the coefficient matrix (see Equation 9) are at the level of machine precision ($\sim 2 \times 10^{-16}$).

In section 3.1, we show the effect of increasing the distance between sources and measurement locations on the predicted source strength and location. As the distance increases, the condition number does not change significantly; in-fact it becomes marginally smaller. However, the relative error in the measurement becomes larger, as the absolute value of the measurement reduce with distance (plume becomes more diluted further away from the source). As a result of this large relative error, the uncertainty in the prediction of source strength and location increases with distance (consistent with Equation 9).

The use of noisy measurement data can result in large uncertainty in the predicted source strength as seen in section 3.2. Large levels of noise result in large relative errors, which in turn results in large uncertainty in source location and strength, consistent with Equation 4). Uncertainty in meteorological variables (shown in section 3.3) such as wind direction or wind speed also results in large uncertainty in the terms of the coefficient matrix $\|\Delta \mathbf{G}\|$, which in turn results in uncertainty in the source prediction.

5   Quantification of Uncertainty due to Noisy Measurement Data

The results shown in Section 4 clearly illustrated that error is introduced in predicting source strength and location due to noisy measurement data or in-correct meteorological data. The goal of this section is to quantify the distribution of this uncertainty and to develop a measurement methodology that reduces the uncertainty. In order to characterize and quantify the measurement uncertainty, we employ a statistical bootstrap procedure discussed below.

5.1   The bootstrap method

The bootstrap was introduced by Efron et al. [27], [28] and is widely used for estimating uncertainty in various applications. Generally speaking, the bootstrap proceeds by re-sampling the observed data with replacement, and the parameters (e.g. $\tilde{\mathbf{Q}}$) are re-computed with the *bootstrap* datasets. After this is done many times, the variability in the bootstrap replicates provide an estimate of the variability in the original parameter estimate.

To begin, we modify Equation 1 so that it explicitly recognizes the measurement error in $\mathbf{C}$.

$$\mathbf{C} = \mathbf{GQ} + \mathbf{C}_{bg} + \epsilon, \tag{10}$$

where ϵ is a random vector with mean vector $\mathbf{0}$ and co-variance matrix $\sigma^2 \text{Diag}(\mathbf{GQ})$, where $\text{Diag}(x)$ is a diagonal matrix with x on its diagonal. Next, define $\tilde{\epsilon} = \mathbf{C} - \mathbf{G\tilde{Q}}$ and $\tilde{\mathbf{r}} = \tilde{\epsilon}/\mathbf{G\tilde{Q}}$, where the

"/" operator implies element-wise division. Now, carry out these steps:

1. Re-sample with replacement the elements of $\tilde{\mathbf{r}}$ to get $\mathbf{r}^*$.

2. Calculate $\boldsymbol{\epsilon}^* = \mathbf{r}^* \times \mathbf{G}\tilde{\mathbf{Q}}$, where the "$\times$" operator implies element-wise multiplication.

3. Calculate $\mathbf{C}^* = \mathbf{G}\tilde{\mathbf{Q}} + \boldsymbol{\epsilon}^*$.

4. Calculate $\tilde{\mathbf{Q}}^*$ by solving the inverse problem using $\mathbf{C}^*$ instead of $\mathbf{C}$.

5. Repeat 1 – 4 B times to get $\tilde{\mathbf{Q}}_1^*, \tilde{\mathbf{Q}}_2^*, \cdots, \tilde{\mathbf{Q}}_B^*$

The bootstrap replicates $\tilde{\mathbf{Q}}_1^*, \tilde{\mathbf{Q}}_2^*, \cdots, \tilde{\mathbf{Q}}_B^*$ are used to summarize the variability in $\tilde{\mathbf{Q}}$. For example, if $\tilde{\mathbf{Q}}(i)$ is the ith element of $\tilde{\mathbf{Q}}$, the standard deviation of $\tilde{\mathbf{Q}}_1^*(i), \tilde{\mathbf{Q}}_2^*(i), \cdots, \tilde{\mathbf{Q}}_B^*(i)$ is an estimate of the standard deviation of $\tilde{\mathbf{Q}}(i)$. Also, the $\frac{\alpha}{2}$ and $1 - \frac{\alpha}{2}$ quantiles of $\tilde{\mathbf{Q}}_1^*(i), \tilde{\mathbf{Q}}_2^*(i), \cdots, \tilde{\mathbf{Q}}_B^*(i)$ are an approximate $(1 - \alpha)100\%$ confidence interval for $\mathbf{Q}(i)$, the true source strength.

To choose B, we take an initial guess, B_0 and run the bootstrap procedure twice. If the difference in the results between the two runs is practically trivial, B_0 is sufficiently large. If not, repeat with a larger value of B until the difference between the two runs is as small as required, i.e. the number of decimal places of accuracy that are required.

5.2   Application of the bootstrap process to estimate uncertainty

The bootstrap iterative process described in section 5.1 was used to iteratively estimate the source strength with various estimates of the measurement vector. The measurement vector was obtained by adding an error vector (difference between the predicted concentrations and measurements) through re-sampling with replacement. Before employing the bootstrap procedure to estimate the variability, it was important to determine the maximum number of iterations that were needed to obtain a converged solution. Figure 12 shows bar plots of the maximum source strength at each index locations at three different points during the evolution of the bootstrap process. Results are shown after 100 bootstrap replications(left panel), 500 bootstrap replications (middle panel) and 1000 replications (right panel). While convergence has not been achieved after 100 replications, comparison between the results for 500 replications and 1000 replications show that convergence has been achieved. Based on Figure 12, results for 1000 replications will be used to quantify uncertainty in the inversion process.

Figure 13 shows a surface plot of the maximum sources strength at each grid point of the rectangular domain, obtained over 1000 replications of the bootstrap procedure. This plot shows the uncertainty in predicting source strength and location due to use of noisy measurement data. Comparison of the bootstrap results shown in Figure 13 with the assumed source distribution shown in Figure 1 indicates that there was considerable uncertainty in the location of the sources. The stronger (leftmost) source "A" as well as the weaker (rightmost) source "B" are visible in the plot shown in Figure 13, but their exact location and strength seems to be unclear. It is important to note that the estimated locations varies along the x-axis, while the variability along the y-axis is relatively small. The results of the bootstrap procedure indicate that the uncertainty in source prediction is not distributed uniformly over the entire domain. Instead the uncertainty is limited to the streamwise direction (in this case the x-direction) for both the sources.

In order to test if the distribution of uncertainty in source identification is limited to the streamwise direction, a set of simulations were conducted where the wind direction was shifted to be parallel to the y-axis (southerly wind). The measurement locations were also shifted so that they were nominally perpendicular to the wind direction. Figure 14 shows a schematic diagram

16
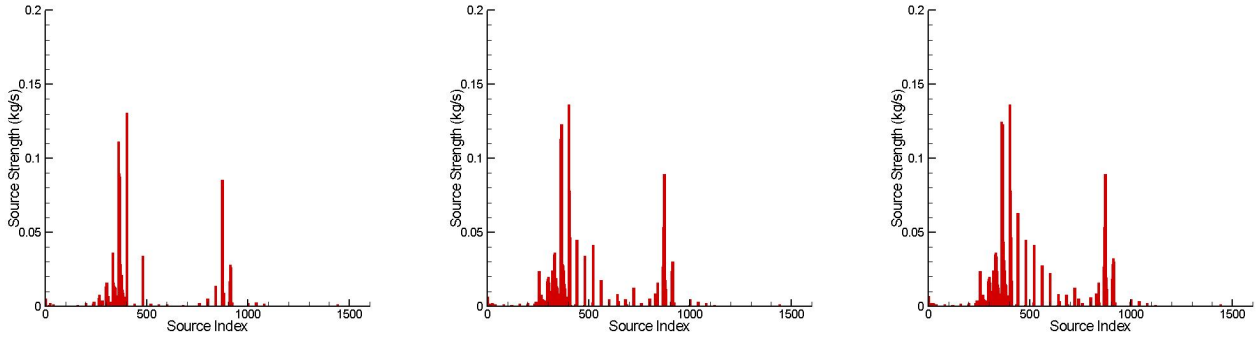
Figure 12: Bar chart showing the maximum source strength plotted as a function of grid index for various levels of iteration. Results are shown for 100 iterations (left sub-figure), 500 iterations (middle sub-figure) and 1000 iterations (right sub-figure).
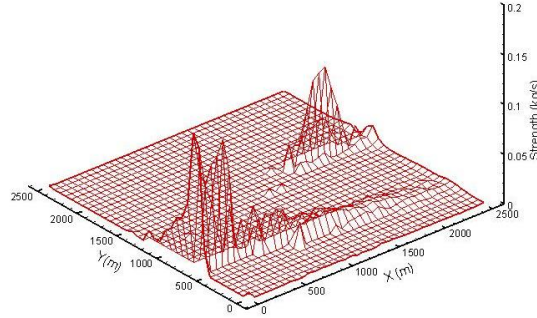

Figure 13: Surface plot showing the maximum source strength at each grid location, plotted at the end of 1000 iterations of a bootstrap method. The wind is parallel to the x-axis.

of the new configuration. The only difference between the configuration shown in figure 14 and the one shown in Figure 1 is the wind direction and the measurement locations. The location of the square source area did not change, nor did the strength and location of the assumed sources A and B. Synthetic data was generated using the plume model Equation 6 to calculate downwind concentrations at the locations illustrated by the lines in Figure 14. As for the previous cases, a wind speed of 2.5 m/s (parallel to the X-axis) and a neutral atmospheric stability (PGT class D, urban) was assumed.

Using only the downwind measurements and the coefficient matrix, $\mathbf{G}$, generated from Equation 6, the nnls algorithm was used to solve the inverse problem by estimating the source vector, $\mathbf{Q}$. The resulting effect of using noisy data on the inverse calculation is illustrated in Figure 15, which shows surface and bar charts for the predicted source distribution. Comparison of the predicted source distribution (Figure 15) and the assumed source distribution (Figure 2) again indicates that there are significant differences in the predicted source strength and location due to the noise in the measurement data. The total predicted source strength was 0.0.2451 kg/s, which is only 3.2% greater than the actual (assumed) source strength. Surface and bar charts (Figure 15) indicate the presence of multiple sources, and the location of the sources was significantly different from the assumed source distribution. Estimates of crosswind locations were accurate for both of the

17
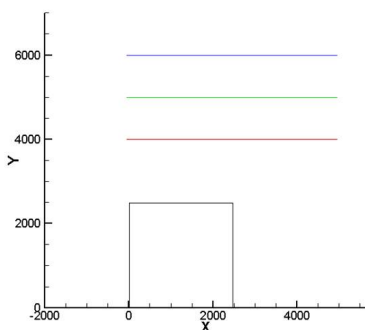
Figure 14: Plan view of the model domain used to investigate the effect of a wind in a direction parallel to the y-axis.

sources, but the streamwise (y-axis) location of the stronger source (source A) was not estimated accurately. Overall, seven source locations were identified in the inverse calculation, though only two sources had strengths of the same order as the true sources.
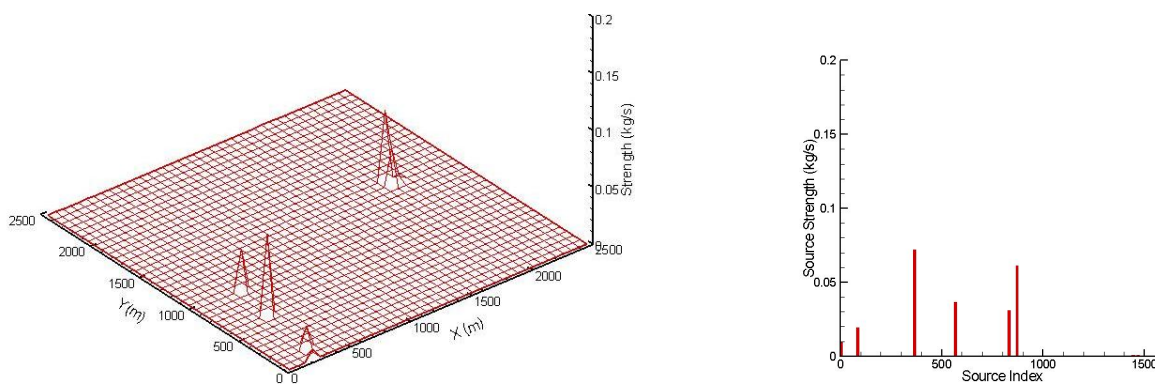
Figure 15: Surface and bar chart showing the location of the predicted sources and their strength, when the wind is parallel to the y-direction.

As for the case when the wind was in the x-direction, we used the bootstrap procedure to quantify the uncertainty for the case when the wind is in the y-direction. Figure 16 shows a surface plot of the maximum source strength over 1000 bootstrap replicates at each grid point of the rectangular domain, assuming that the wind was in the y-direction. Results indicate that that the stronger (leftmost) source "A" as well as the weaker (rightmost) source "B" are visible in the plot shown in Figure 16, but their location and strength is not clear. It should be noted that the uncertainty in the location of the sources and the variability is primarily in the y-direction (streamwise), while the variability in the x-direction is relatively small. Results of the bootstrap procedure with a wind in either the x or y-direction, both indicate that the uncertainty in source prediction is primarily in the streamwise direction. This is an important conclusion, and is the basis for designing a measurement methodology aimed at reducing the uncertainty in source prediction, as discussed in the next section.

18
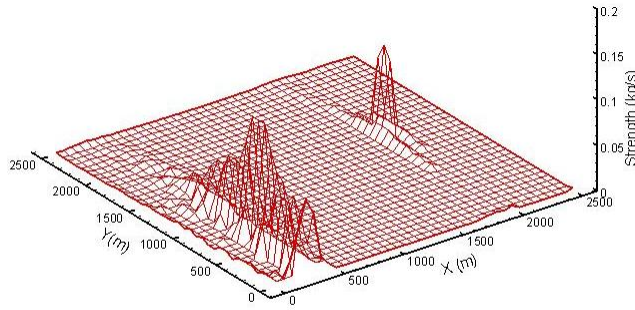
Figure 16: Surface plot showing the maximum source strength at each grid location, plotted at the end of 1000 iterations of a bootstrap method. The wind is parallel to the y-axis.

6   A Novel Measurement Methodology for Reducing the Uncertainty in Source Prediction

In this section we propose a new measurement methodology for reducing the uncertainty introduced in the source prediction due to noisy data. The application of the bootstrap procedure demonstrated the uncertainty in source strength and location when the wind was in the +x-direction (Figure 13), or in the + y-direction (Figure 16). Results clearly illustrated that the uncertainty is distributed in the streamwise direction.

In order to reduce this uncertainty, we investigate the feasibility of taking data from two different wind directions and combining them together in a single calculation. Figure 17 (left sub-figure) illustrates a typical configuration for collecting data with two different wind directions. The set of measurement lines parallel to the y-axis, were used to collect data when the wind was blowing in the +ve x-direction. The set of measurement lines parallel to the x-axis were used to collect data when the wind was in the +y-direction. For each wind direction, synthetic data was generated on the measurement lines using an assumed source distribution shown in Figure 2. Note, that the source area and the location / strength of the assumed sources has not changed in any of these configurations. Next, we introduced 10% noise in the measurement data collected at each location for both the wind directions. The noisy measurement data from the two wind directions is combined into a single data set and is used for inversion. It should be pointed out that there is twice as much data available for inversion as compared to the earlier cases. The inversion approach was similar to the one discussed in the previous section, the primary difference being that the data from two different wind directions was combined in one single calculation.

Figure 17 (right sub-figure) shows the results of the inversion process, where synthetic data with noise from two different wind directions was utilized. Comparison of the predicted source strength and location following the inversion process (Figure 17 right sub-figure) and the assumed source distribution (Figure 2), indicates that the results are quite similar. The total source strength predicted from the inversion process was computed at 0.2333 kg/s, which compared favorably with the total assumed source strength of 0.2373 kg/s. Moreover, the location of the predicted sources also compared favorably with the assumed source distribution. The bootstrap process (described in section 5.1) was used again on the configuration described in Figure 17 (left sub-figure) to quantify the variability and uncertainty in source location and strength. Figure 18 left sub-figure) shows the maximum source strength and location over 1000 bootstrap replications, while Figure 18 right sub-figure shows the minimum source strength and location over 1000 iterations. The same data is

19

shown in bar format in Figure 19.
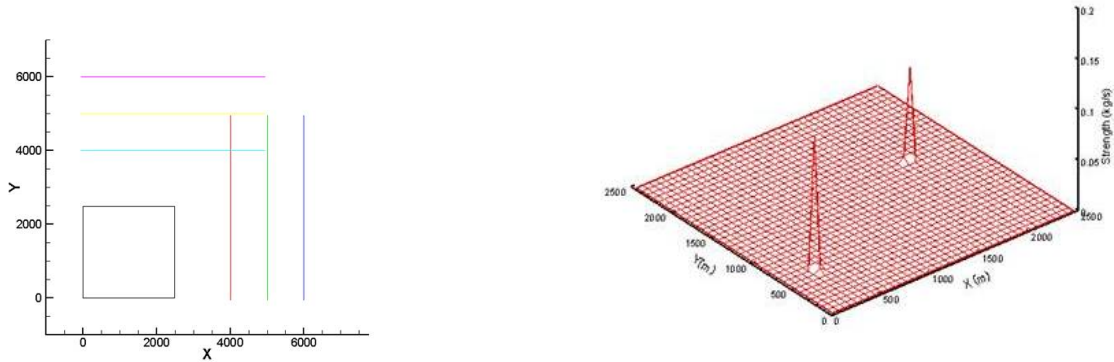
Figure 17: Left sub-figure shows a plan view of the source-sensor configuration that was used for estimating and reducing the uncertainty in prediction of sources and their location. Data from two different wind directions was utilized. The right sub-figure shows a surface plot of the predicted source distributions obtained when noisy data (synthetic data with 10% noise) from two different wind directions was combined in a single inversion step.
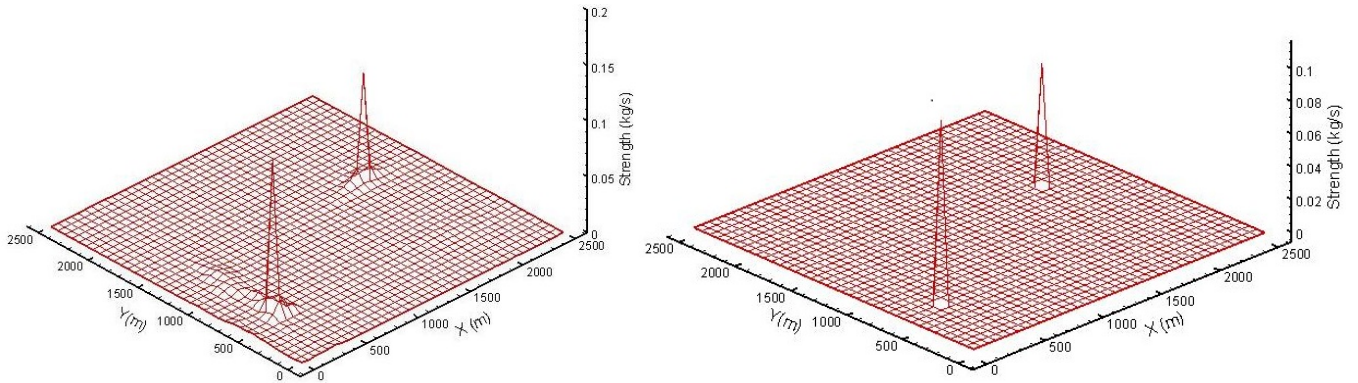

Figure 18: Results of the bootstrap procedure when noisy measurement data from two different wind directions are used in a single inversion procedure. The left sub-figure shows surface plot of the maximum predicted values over 1000 iterations, while the left sub-figure shows a surface plot of the minimum values.

These results clearly demonstrate that the uncertainty due to noisy measurement data can be reduced by using measurements from two different wind directions combined together as part of a single inversion procedure. In general, the best results are obtained under conditions when the two wind directions are perpendicular to each. However, it should be noted that the two wind directions do not have to be perpendicular to each other, and that the analysis can be conducted with the two winds at a non-right angle to each other. Furthermore, utilizing data from more than two different wind directions can further reduce uncertainty in the analysis.

It should also be pointed out that collecting data for two different wind directions is not very challenging, since the mean wind speed and direction changes several times during the course of a single day. As a result collecting data from two or more wind directions / speed is not a significant issue, as long as appropriate roads are available for collecting downwind data. Moreover, the

20

Figure 19: Results of the bootstrap procedure when noisy measurement data from two different wind directions are used in a single inversion procedure. The left sub-figure shows a bar plot of the maximum predicted values over 1000 iterations, while the left sub-figure shows a bar plot of the minimum values.

reduction in uncertainty (shown in this section) is due to the presence of wind data in two different directions, and not due to the availability of more data. This was confirmed by reducing (halving) the number of measurement points, and finding no change in the computed results or the reduction in uncertainty. The approach for reducing uncertainty is also independent of the model used for plume dispersion, and as a result is applicable for all scenarios where one needs to estimate source location and strength from measurement data.

7 Conclusions and Suggestions for Future Research

Recent development of accurate instruments for measuring greenhouse gas concentrations and the ability to mount them in ground-based vehicles has provided an opportunity to make temporally and spatially resolved measurements in the vicinity of suspected source locations. The basic approach of using downwind atmospheric measurements in an inversion methodology to predict source strength and location can be an ill-posed problem and results in high degree of uncertainty, if the wrong measurement methodology is used.

In this report, we have presented a new measurement strategy for reducing the uncertainty in predicting source strength and location from downwind measurements. In order to demonstrate the approach, the basic inversion methodology built around a plume dispersion model was presented. Synthetic data derived form an assumed source distribution was used to allow us to compare and contrast the predicted source strength and location. The effect of introducing various levels of noise in the synthetic data on the inversion methodology was presented. It was concluded that the presence of noise in synthetic data resulted in large uncertainty in the location of the sources. The use of noisy measurement data had a small effect on the total predicted source strength, but gave rise to several spurious sources (in many cases 8-10 sources were detected, while the assumed source distribution only consisted of 2 sources). Uncertainty in wind direction also resulted in large uncertainty in the location of the predicted sources. Similar results were obtained when uncertainty in determining the meteorological variables was incorporated in the inversion process. The new measurement strategy involved collecting data from two or more wind directions. The data is subsequently combined together as part of a single inversion process. Results of the bootstrap procedure indicated that the uncertainty in locating sources reduced significantly when data from

21

two or more wind directions is used simultaneously.

Future research will involve collecting data as part of a mobile measurement campaign around suspected methane sources such as landfills, natural gas transmission and regulating stations, and waste-water treatment plants. The measurement methodology presented in this report will be incorporated as part of the mobile campaign to accurately identify sources and their strength. Such approaches can be very useful in developing an emissions inventory for mega cities and for evaluating the role of remediation measures on greenhouse gas emissions.

8 Acknowledgments

References

[1] Gerbig, C., J. C. Lin, S. C. Wofsy, B. C. Daube, A. E. Andrews, B. B. Stephens, P. S. Bakwin, and C. A. Grainger, Toward constraining regional-scale fluxes of CO2 with atmospheric observations over a continent: 1. Observed spatial variability from airborne platforms, J. Geophys. Res., 108(D24), 4756, doi:10.1029/2002JD003018, 2003.

[2] Gerbig, C., J. C. Lin, S. C. Wofsy, B. C. Daube, A. E. Andrews, B. B. Stephens, P. S. Bakwin, and C. A. Grainger, Toward constraining regional-scale fluxes of CO2 with atmospheric observations over a continent: 2. Analysis of COBRA data using a receptor-oriented framework, J. Geophys. Res., 108(D24), 4757, doi:10.1029/2003JD003770, 2003.

[3] Kort, E. A., W. M. Angevine, R. Duren, and C. E. Miller (2013), Surface observations for monitoring urban fossil fuel CO2 emissions: Minimum site location requirements for the Los Angeles megacity, J. Geophys. Res. Atmos., 118, doi:10.1002/jgrd.50135.

[4] Zhao, C., A. E. Andrews, L. Bianco, J. Eluszkiewicz, A. Hirsch, C. MacDonald, T. Nehrkorn, and M. L. Fischer (2009), Atmospheric inverse estimates of methane emissions from Central California, J. Geophys. Res., 114, D16302, doi:10.1029/2008JD011671.

[5] Gurney, K.R., Razlivanov, I., Song, Y. Zhou, Y., Benes, B., M. Abdul-Massih (2012): Quantification of fossil fuel CO2 at the building/street scale for a large US city, Environmental Science and Technology, dx.doi.org/10.1021/es3011282

[6] Cambaliza, M.O., P.B. Shepson, D. Caulton, B. Stirm, D. Samarov, K. Gurney, J. Turnbull, K.J. Davis, A. Possolo, A. Karion, C. Sweeney, B. Moser, A. Hendricks, T. Lauvaux, K. Mays, J. Whetstone, J. Huang, I. Razlivanov, N. Miles, and S.J. Richardson: Assessment of uncertainties of an aircraft-based mass-balance approach for quantifying urban greenhouse gas emissions. In preparation.

[7] Miles, Lauvaux, Davis, Richardson, Sarmiento, Wu, Karion, Sweeney, Vimont, Turnbull, Hardesty, Brewer, Gurney, Razlivanov, Iraci, Hillyard, Shepson, Cambaliza, Whetstone. Dectection and quantification of urban greenhouse gas emissions: Results from the INFLUX project. Presented at the 42nd NOAA ESRL Global Monitoring Annual Conference, Boulder, CO, 20 May . 21 May 2014.

[8] E. Yee, T. K. Flesch. Inference of emission rates from multiple sources using Bayesian probability theory. J. Environ. Monit. 12:622-634, 2010.

[9] Carbon Cycle Uncertainty in Regaional Carbon Cycle Assessment and Processes (RECCAP) I. G. Enting, P. J. Rayner, P. Ciais, Biogeosciences, 9, 2889.2904, 2012.

[10] B. P. Crenna, T. K. Flesch, J. D. Wilson. Influence of source-sensor geometry on multi-source emission rate estimates. Atmospheric Environment 42:7373-7383 (2008).

[11] T. K. Flesch, L. A. Harper, R. L. Desjardins, Z. Gao, B. P. Crenna. Multi-source emission determination using an inverse-dispersion technique. Boundary-Layer Meteorol. 132:11-30 (2009).

[12] T. K. Flesch, J. D. Wilson, E. Lee. Backward-time Lagrangian stochastic dispersion models and their application to estimate gaseous emissions. J. of Applied Meteorology 34:1320:1332 (1995).

[13] L. C. Thomson, B. Hirst, G. Gibson, S. Gillespie, P. Jonathan, K. D. Skeldon, M. J. Padgett. An improved algorithm for locating a gas source using inverse methods. Atmospheric Environment 41:1128-1134 (2007).

[14] E. Lushi, J. M. Stockie. An inverse Gaussian plume approach for estimating atmospheric pollutant emissions from multiple point sources. Atmospheric Environment 44:1097-1107 (2010).

[15] H.-J. Jeong, E.-H. Kim, K.-S. Suh, W.-T. Hwang, M.-H. Han, H.-K. Lee. Determination of the source rate released into the environment from a nuclear power plant. Radiation Protection Dosimetry 113:308-313 (2005).

[16] A. C. Rudd, A. G. Robins, J. J. Lepley, S. E. Belcher. An inverse method for determining source characteristics for emergency repsonse applications. Boundary-Layer Meteorol. 144:1-20 (2012).

[17] Crosson, E.R., 2008. A cavity ring-down analyzer for measuring atmospheric levels of methane, carbon dioxide, and water vapor. Applied Physics B: Lasers and Optics 3, 403-408.

[18] N. De Nevers. Air pollution control engineering. 2nd ed. McGraw-Hill (2000).

[19] Alvarez, R.A., Pacala, S.W., Winebrake, J.J., Chameides, W.L., Hamburg, S.P., 2012. Greater focus needed on methane leakage from natural gas infrastructure. Proceedings of the National Academy of Sciences U.S.A. 109, 6435e6440.

[20] Ermak, D.L., 1977. An analytical model for air pollutant transport and deposition from a point source. Atmospheric Environment 11 (3), 231-237.

[21] R. F. Griffiths. Errors in the use of the Briggs parameterizations for atmospheric diffusion coefficients. Atmospheric Environment 17:2861-2865 (1994).

[22] J. S. Irwin, A Theoretical Variation of the Wind Profile Power-Law Exponent as a Function of Surface Roughness and Stability, Atmospheric Environment 13:191-194 (1979).

[23] C. L. Lawson, R. J. Hanson. Solving Least Squares Problems. Society for Industrial and Applied Mathematics, Philadelphia, 1995.

[24] http://www.netlib.org/lawson-hanson/all

[25] D. C. Lay. Linear algebra and its applications. 2nd ed. Addison Wesley (2000).

[26] Handbook of Linear Algebra. *Edited by* L. Hogben. Taylor & Francis Group 2007.

[27] B. Efron. Bootstrap Methods: Another Look at the Jackknife. The Annals of Statistics 7:1-26 (1979).

[28] B. Efron, R. J. Tibshirani. An Introduction to the Bootstrap. Chapman & Hall (1993).

24

List of Figures